RISK FACTORS OF RADIOTHERAPY-INDUCED CEREBRAL MICROBLEEDS AND SERIAL ANALYSIS OF THEIR SIZE COMPARED TO WHITE MATTER CHANGES: A 7T MRI STUDY IN 113 ADULT PATIENTS WITH BRAIN TUMORS

Melanie A. Morrison, Ph.D.[1], **Christopher P. Hess, M.D., Ph.D**[1], **Jennifer L. Clarke, M.D.**[2], **Nicholas Butowski, M.D.**[2], **Susan M. Chang, M.D.**[2], **Annette M. Molinaro, PhD.**[2], **Janine M. Lupo, Ph.D.**[1,3]

[1]Department of Radiology and Biomedical Imaging, University of California San Francisco, San Francisco, CA, USA

[2]Department of Neurological Surgery, University of California San Francisco, San Francisco, CA, USA

[3]UCSF/UCB Graduate Group in Bioengineering

Abstract

Background: Although radiation therapy contributes to survival benefit in many brain tumor patients, it has also been associated with long-term brain injury. Cerebral microbleeds (CMBs) represent an important manifestation of radiation-related injury.

Purpose: To characterize the change in size and number of CMBs over time and to evaluate their relationship to white matter structural integrity as measured using diffusion MRI indices.

Study Type: Longitudinal, retrospective, human cohort.

Population: 113 brain tumor patients including patients treated with focal radiotherapy (n=91, 80.5%) and a subset of non-irradiated controls (n=22, 19.5%).

Field Strength/Sequence: Single and multi-echo susceptibility-weighted imaging (SWI) and multi-band, shell, and direction diffusion tensor imaging (DTI) at 7T.

Assessment: Patient were scanned either once or serially. CMBs were detected and quantified on SWI images using a semi-automated approach. Local and global fractional anisotropy (FA) were measured from DTI data for a subset of 35 patients.

Statistical Tests: Potential risk factors for CMB development were determined by multivariate linear regression and using linear mixed-effect models. Longitudinal FA was quantitatively and qualitatively evaluated for trends.

Correspondence to Janine M. Lupo, Byers Hall UCSF, Box 2532, 1700 4th Street, Suite 303D, San Francisco, CA 94158-2330, USA, Tel: +1 (415) 502-0646; fax: +1 (415) 514-1028; janine.lupo@ucsf.edu.

Results: All patients scanned at 1 or more years post-RT had CMBs. A history of multiple surgical resections was a risk factor for development of CMBs. The total number and volume of CMBs increased by 18% and 11% per year, respectively, though individual CMBs decreased in volume over time. Simultaneous to these microvascular changes, FA decreased by a median of 6.5% per year. While the majority of non-irradiated controls had no CMBs, four control patients presented with fewer than 5 CMBs.

Data Conclusion: Identifying patients that are at the greatest risk for CMB development, with its likely associated long-term cognitive impairment is an important step towards developing and piloting preventative and/or rehabilitative measures for patients undergoing RT.

INTRODUCTION

While radiation therapy (RT) remains a standard treatment for both adult high-grade gliomas, and in low-grade gliomas, it is often associated with long-term side effects including neurocognitive decline[1], leukoencephalopathy[2], radiological evidence of vascular brain injury,[3] and deep and periventricular white matter alterations[4]. With current treatment strategies, the median survival of a lower grade glioma can be as high as 10 years[5], thus minimizing the deficits incurred through treatment becomes important for this patient population.

RT-induced vascular injury typically manifests as variably sized hemosiderin deposits in the brain, termed cerebral microbleeds (CMBs). These can be detected with Susceptibility-Weighted Imaging (SWI) as early as 8 months following treatment, though in most adult patients the onset of vascular injury is usually observed 2 years post-RT.[6] Prior smaller studies have shown increases in the formation of CMBs over time in patients treated with RT for malignant gliomas that were spatially dependent on the RT dose[7], and an absence of CMBs in patients treated with chemotherapy alone.[8] One of the largest and most comprehensive studies to date in adult survivors of childhood brain tumors reported increases in total CMB burden with accumulated time since RT and with greater spatial extent of treatment.[9] Patients treated at a younger age or with an anti-angiogenic drug at the time of recurrence were also found to be at higher risk for CMB development following treatment. When related to neurocognitive measures, CMB burden was associated with impairments in multiple domains of cognitive function, suggesting that CMBs may serve as a potential marker of cognitive impairment.[9] Although this relationship has yet to be shown for patients who received treatment for a brain tumor during adulthood, similar forms of vascular injury have been related to the cognitive decline experienced by healthy aging adults, stroke patients, and patients with neurodegenerative disorders.[10]

While the outcomes of prior studies provide valuable insights into the potential clinical relevance of RT-induced CMBs and the impact that clinical and treatment parameters may have on their development, these prior studies have predominately used lower-field MRI

systems and less sensitive imaging data that results in reduced visualization of CMBs[11], thereby warranting further investigation with more advanced methods. Little published research exists characterizing CMBs, their prevalence, and risk factors in brain tumor patients treated with RT during adulthood. To date, these topics have only been investigated on lower field strength systems with less sensitive imaging in adult survivors of childhood brain tumors[9] for whom age, treatment strategy, and overall disease prognosis and characteristics are markedly different from that of adult brain tumors patients.

The current study takes advantage of 7 Tesla MRI to examine (i) the incidence of CMBs in those patients treated with versus without RT (ii) risk factors for CMB development following treatment with a focal RT regimen and (iii) changes in CMB size, total burden, and WM structure over time with serial imaging.

MATERIALS AND METHODS

Patient Recruitment

With approval from our Institutional Review Board, charts and imaging from 133 adult patients with brain tumors who had provided informed written consent to participate in research scan development between 2006 and 2017 were retrospectively reviewed for this study. Inclusion criteria included: diagnosis of an adult brain tumor (preferably an adult glioma, 2007 World Health Organization (WHO) grading I-IV) no other major neurological or neurovascular disorders, and adequate quality imaging data to permit analysis. A subset of non-irradiated patients, treated either with surgery alone or a combination of surgery and chemotherapy, were included to form a control group. The final analysis included 113 out of 133 patients ($n = 91$ who had received RT at least 2 months prior to imaging and $n = 22$ non-irradiated controls), after the exclusion of 20 patient datasets due to motion-related artifacts. Patient demographics for the 113 included patients are listed in Table 1.

MRI Acquisition

All patients were scanned on 7-Tesla GE scanner with a two channel transmit coil containing a 32 channel receive coil inset either once or for 2-8 serial scans with varying scan intervals. SWI data were acquired either using a single-echo sequence[13] (spoiled gradient echo, flow compensation along readout, TR/TE=50/16ms, FA=20, with 2mm slice thickness, 0.5 mm in-plane resolution, 24cm FOV, parallel imaging with R=3) or a newer multi-echo sequence that enabled the simultaneous collection of SWI and Time-of-Flight MR angiography data (a multi-slab, multi-gradient echo, flow compensation along readout, FA=20, TR/TE1/TE2/TE3/TE4= 40/2.7/10.5/13.2/20.9ms, with 1mm slice thickness, 0.5 mm in-plane resolution, 24cm FOV, parallel imaging with R=3).[12] SWI post-processing as described in Lupo et al[13] and Bian et al[12] were used to generate the final images from the raw data. T1-weighted images of brain anatomy were also acquired during the same session; an inversion recovery, spoiled gradient recalled (IR-SPGR) pulse sequence and/or MP2RAGE pulse sequence were acquired (TI/TR/TE = 600ms/6s/2ms, FA=8, with 1mm isotropic resolution, 25.6cm FOV, and parallel imaging with R=2.2). Multi-band, shell, and direction diffusion-tensor imaging (DTI)[14] was performed for 35 patients (spin echo planer readout, with 3 simultaneously acquired slices per excitation, TR/TE=5s/70ms, with 2mm

isotropic resolution, 25.6cm FOV, 30 directions at b=1000s/mm^2, and 60 directions at b=2000s/mm^2, & in plane parallel imaging R=2). Fractional anisotropy (FA) maps were generated from the 30 directions of the b=1000 scans using FSL's "dtifit" toolbox (FMRIB, Oxford, UK). A top-up correction was first performed using all directions and b-values.

Microbleed Detection

CMBs were detected using a semi-automated CMB detection algorithm[15], recently updated to improve specificity and perform CMB volume quantification[16]. The MATLAB (Natick, MA, USA) algorithm accepts a non-projected stack of SWI images, from which it identifies all putative CMB candidates before using hand-crafted features and user-guided classification to differentiate true CMBs from hard mimics associated with vessel architecture. The final candidates are segmented using an iterative thresholding approach and saved as a binary mask that can be overlaid onto the SWI images (Fig. 1C). A summary report is then generated, providing details of CMB counts and volumes.

For patients with serial scans (N=19), the algorithm was applied separately to each SWI dataset. An intensity normalization step ensured standardized conditions for detecting CMBs across serial imaging.

Analysis of Serial Changes

To evaluate changes in CMB size, individual CMBs were randomly selected from serial scan data, such that a percent volume change could be calculated between the initial and final CMB volumes. Global and local FA, indicative of WM changes, were also quantified serially and analyzed for trends. We used an FA threshold of 0.2 to exclude non-WM voxels; global mean and median FA were quantified across the whole brain, while local measures were evaluated within ring-like regions of interest generated via a dilation of individual CMB foci followed by a subtraction of the CMB mask.

Statistical Analysis

To identify potential risk factors for CMB development, we first performed a series of univariate Poisson regressions, with total CMB count as the dependent variable. A Poisson regression was deemed appropriate for this analysis given the gradual unpredictable onset of CMBs. Variables of interest included: sex, race, tumor pathology, primary tumor location, treatment with RT, additional RT due to recurrence, age at time of RT, time since RT in years, maximum brain radiation measured in gray, treatment with chemotherapy, surgical resection, additional surgeries due to recurrence, and type of SWI acquired (single-echo or multi-echo SWI). For those patients irradiated multiple times due to tumor recurrence, measures of age and time since RT were calculated from the first date of brain radiation exposure. Variables that were at least weakly associated with CMB development (P < 0.2) in the univariate model were included in the multivariate model, with sex, race, and age at time of RT included as covariates.

In the sub-set of patients with serial imaging, linear mixed-effects models were employed to relate serial changes in total CMB number and volume as well as in individual CMB size to time since RT using the same covariates.

RESULTS

Frequency of Microbleeds

All patients scanned at 1 or more years post-RT had CMBs. Figure 1A, B illustrates the relationship between total CMB burden and time since RT; one patient presented with many as 250 CMBs at approximately 15 years post-treatment. In the non-irradiated control group, 4 of 22 patients between the ages of 40 and 65 had evidence of 5 or fewer CMBs on MRI.

Risk Factors for Microbleed Development

In the univariate analysis, time since RT, multiple surgical resections, tumor pathology, and type of SWI acquisition, were associated with increased CMB development (Table 2). Maximum brain radiation dose received was not associated with increased CMB development.

In the multivariate analysis, all variables remained significant except for type of SWI acquired (Table 2). With each additional year following treatment, the data showed an approximate 10% increase in CMB burden (rate ratio: 1.10, CI [1.04, 1.16]). Patients who underwent multiple resections developed CMBs at a rate 2.42 times greater than those patients who had only one intervention (rate ratio: 2.42, CI [1.36, 4.30]); there was no significant difference in time elapsed since treatment for these two groups. The rate of CMB development was greater for patients diagnosed with WHO grade III anaplastic astrocytomas when compared to a WHO grade IV glioblastoma diagnosis (rate ratio: 2.41, CI [1.21, 4.77]), while patients with other pathological diagnoses developed CMBs at a much lower rate than patients with glioblastoma (rate ratio: .257, CI [.064, 1.04]). Frontal lobe tumors were associated with increased rates of CMB development in comparison to temporal and parietal tumors (rate ratios: .445, CI [.213, .932]; .204, CI [.046, .900]). Patients with occipital, cerebellum or brainstem tumors, however, developed CMBs at 3.58 times the rate of patients with frontal lobe tumors (rate ratio: 3.58, CI [1.20, 10.6]). Although not significant in the multivariate analysis, in the univariate analysis, single-echo SWI was associated with fewer CMBs when compared to multi-echo SWI (rate ratio: .534, CI [.291, .980]) as expected.

Serial Microbleed and White Matter Changes

All irradiated patients imaged at 2 or more timepoints demonstrated serial increases in total CMB burden. The total number and volume of CMBs significantly increased by 18% and 11% per year (rate ratios: 1.18, CI [1.14, 1.22]; 1.11, CI [1.09, 1.13]), respectively (Fig. 1B). Individual CMBs however, showed significant decreases in volume, irrespective of their initial volume or time since RT, at a rate of −25% per year (rate ratio: .75, CI [.70, .81]) (Table 3, Fig. 2). Some CMBs even disappeared altogether. Simultaneous to these vascular changes, global FA values showed declines ranging between 1.3% and 21.4% per year (median, 6.5%) (Fig. 3). Local FA followed the same trend (Fig. 4).

DISCUSSION

In this study, we showed that 100% of patients scanned at 1 or more years post-RT presented with one or more CMBs. Previously it has been shown using SWI at 7T, high incidence rates for CMB formation in glioma patients at 2-years after RT.[8] Failure to detect CMBs prior to 2-years in this earlier study, may be due to the fact that manual CMB labelling was performed in the absence of computer aid, lower resolution acquisitions with less coverage, and the overall lack of available scans within that time period. Computer-based CMB detection algorithms have shown great success in their ability to identify smaller, low-contrast CMBs that are often overlooked by human raters.[14] van den Heuvel et al reported an average sensitivity of 77% based on manual detection by six experts, that increased to 93% with the aid of a guided user interface.[17] The implementation of our semi-automated, user-guided CMB detection algorithm in this study[12], likely enhanced our ability to detect CMBs earlier on.

Another group had recently investigated CMB prevalence in low-grade glioma patients using ultra high-field MRI techniques, also demonstrating consistent CMB presence after treatment with RT.[18] In younger brain tumor populations, the majority of published data is based on less sensitive imaging data (T2* magnitude images) and/or clinical 1.5T and 3T systems, which have a known reduced sensitivity for CMBs compared to SWI images and 7T MRI where the susceptibility effect is greater and CMB contrast is heightened[11]. Consequently, lower incidence rates have been reported in the literature. For example, Roddy et al reported in their study of 149 adult survivors of childhood brain tumors, cumulative incidence rates of 10.8% after 1 year and 48.8% a 5-years post-RT, with a maximum of 49 CMBs detected in any one patient.[9] Another study of the same population reported an incidence rate of 44% (n=93) based on a median follow-up of 5.8 years.[19] Roongpiboonsopit et al investigated the prevalence of CMBs in younger adults (median age 28.8 years) treated with whole-brain RT for a medulloblastoma; they identified CMBs in 67% (n=18) of patients followed for a median of 4.1 years.[20] In our recent experience, in an ongoing study using the same methods as in the present study to assess CMB prevalence in adult survivors of pediatric medulloblastomas, we have so far observed a 100% cumulative incidence rate for CMB formation at follow-up times ranging between 1.1 and 15.5 years (median, 6.2 years). This supports early and accurate detection of RT-induced CMBs using advance imaging and post-processing methods.

While the majority of non-irradiated controls presented without CMBs, 18.1% were found to have 5 or fewer CMBs. This observation agrees well with prior studies investigating the prevalence of CMBs in healthy aging adults. The Rotterdam study found that in non-demented adults aged 45 years and older, 609 subjects (15.3%) had at least one CMB on MRI.[21] Only 71 (11.7 %) of subjects with evidence of CMBs presented with 5 or more CMBs, indicating that the presence of many CMBs is relatively rare in the healthy aging population. In our study, we were unable to differentiate age-related CMBs from RT-associated CMBs since no baseline 7T SWI imaging was performed prior to RT. Nonetheless, CMBs were observed as early as 1-year post-treatment in patients younger than 45 years, who typically do not present with CMBs otherwise.[21] Nearly all patients scanned at 2 or more years following RT presented with abnormal quantities of CMBs that could not

be attributed to aging alone. Since a high burden of CMBs has been associated with worsening cognitive performance,[21] identifying those patients at risk for developing a substantial number of CMBs after RT is an important first step towards strategizing early preventative and/or rehabilitative measures.

In our multivariate analysis, exposure to multiple surgical resections was a strong risk factor for CMB development. Patients who had experienced tumor recurrence requiring a second or third surgical intervention, were more likely to develop CMBs than patients who had only one surgery. To our knowledge, CMB development has not yet been linked to surgical resection alone, though some have reported the appearance of new CMBs, even in children, following endovascular surgery.[22] Although the pathophysiology of RT-induced vascular injury remains unclear, it appears as though surgery adds further stress to already compromised vascular integrity, subsequently accelerating the mechanism through which CMBs form over time.

Maximum brain radiation, even when accounting for multiple RT treatments, was not a significant risk factor for CMB development. Roddy et al found a similar result in their analysis using a maximum dose approximation. These negative findings likely reflect the unsuitability of this measure for patients treated with focal RT since the dose is distributed non-uniformly and the spatial extent varies with tumor volume. The volume of the higher dose region should be a more appropriate metric for evaluation, as Wahl et al[7] in 2017 found significantly more CMBs in this region in the first 3 years following RT. Unfortunately, radiation dosimetry maps were not available for enough patients included in our analysis to appropriately assess associations between CMB development and dosimetry volumes and/or the extent of treatment.

Specific tumor pathologies and tumor locations were also linked to more severe cases of RT-induced injury in our analysis. A WHO grade III, anaplastic astrocytoma was associated with an increased rate of CMB development when compared to a WHO grade IV glioblastoma. This observation at the univariate level could be due to differences in survival between the two grades, however, the multivariate analysis with covariates demonstrated a similar incidence rate ratio, suggesting there is perhaps an underlying biological factor or some other combination of factors driving this difference.

The range of follow-up times for patients with diagnoses belonging to the "other" group (including meningioma, ependymoma, chordoma, choroid plexus papilloma, hemangioblastoma, and ganglioma) exceeded 2 years, yet patients treated for a glioblastoma or an anaplastic astrocytoma were likely to develop CMBs at an increased rate. One hypothesis is that high-grade gliomas are treated more aggressively than other tumor diagnoses due to their high probability for recurrence.

In regard to tumor location, occipital, cerebellum and brainstem tumors combined were associated with the highest rate of CMB development, while frontal lobe tumors were associated with increase rates of development compared to temporal and parietal lobe tumors. This finding suggests that the posterior brain and frontal lobe are the most

radiosensitive brain regions in adults, agreeing well with previous findings in pediatric populations.[9,20]

Despite a steady increase in the total number and volume of CMBs in the years following RT, results from this study demonstrate that CMBs are decreasing in size over time, possibly by way of blood product breakdown over many years[23]. A previous report showed possible instances of increasing CMB volume based on qualitative evaluation of serial imaging during initial formation at 14 and 16 months post-RT[6], however the majority of CMBs when reassessed with quantitative measures during longer follow up periods were found to be decreasing in volume.

Similar changes in CMB volume have previously been reported during the acute and chronic phases following a traumatic brain injury.[24,25,26] Liu et al found a dramatic decrease in quantitative measures of CMBs from serial imaging acquired beyond 2 years post-injury[24], while Lawrence et al and Watanabe et al reported the appearance of CMBs within the first few hours following injury; CMBs showed reductions in volume over a 2-15 day period that were associated with patient recovery[25,26]. Thus, identifying treatment strategies to accelerate the mechanism through which CMBs decrease in size may be a viable alternative for minimizing CMB-associated deficits.

Simultaneous to vascular injury, our results provide evidence for RT-induced neuronal damage not only across the whole-brain, but within local regions surrounding CMB foci. WM FA changes suggest decreases by as much as 21.4% per year, which exceeds typical FA changes in adults that are associated with natural aging of the brain[27]. Prior studies have also shown evidence of progressive WM damage after RT in adults[28,29], as well as immediate changes following the completion of RT when CMBs are typically not yet detected[30]. Mabbott et al showed RT-induced reductions in FA in children were associated with worse intellectual outcome when compared to control subjects[31], potentially suggesting that there may be a relationship between FA and CMBs, though no measures of the latter were considered in their study. In our data, there were no direct correlations between total CMB burden and the magnitude of FA or change in FA, however, serial DTI was only performed for a small sub-set of patients. Future work will aim to more thoroughly investigate the relationship between CMBs, WM damage, and cognition.

In addition to aforementioned limitations, imaging data that were included in our analysis were acquired at a single time-point for the majority of patients, thus making it unclear as to when CMBs first developed. Of the patients that did undergo longitudinal imaging, the data were limited.

SWI images were acquired with two different sequences resulting in two different slice thicknesses; however, all scans analyzed from the same patient however were acquired with the same sequence. The multi-echo sequence[12] required a 1-mm thick slice for the first echo used for MR angiography, while the prior single-echo sequence[13] was performed at 2-mm slice thickness to balance SNR, vessel contrast, and scan time. The reduced resolution of the latter acquisition limited our ability to accurately detect CMBs with small radii (<2mm); this was also evident in our univariate analysis. Biases in patient selection associated with

retrospective study designs may also pose as a limitation. To minimize this, we utilized all 7T imaging data that was available in our database, only discarding those datasets with motion-related artifacts and not excluding patients based on clinical factors beyond the requirement of treatment with RT. Last, our analysis did not assess the relationship between CMBs and neurocognitive outcome as there were no standardized protocols in place to measure cognitive function when the study initiated. In general, it is difficult to differentiate cancer-related cognitive impairment from treatment-related cognitive impairment for this population who experience high levels of recurrence. Nonetheless, the breadth of evidence in the literature demonstrates a relationship between CMBs and neurocognitive impairment in other adult populations.[11]

In conclusion, we have shown that CMBs are prevalent in all adult patients treated with RT for a brain tumor. Despite decreasing in size over time, their number increases overtime, at a rate which is associated with both the total number of surgical interventions undergone and the primary tumor location. Identifying patients that are of greatest risk for CMB development and associated long-term cognitive impairment is an important step towards developing and piloting various preventative and/or rehabilitative measures.

ACKNOWLEDGEMENTS

REFERENCES

1. Greene-Schloesser D, Robbins ME, Peiffer AM, Shaw EG, Wheeler KT, & Chan MD (2012). Radiation-induced brain injury: A review. Frontiers in Oncology, 2(7), 73. [PubMed: 22833841]

2. Monaco EA, Faraji AH, Berkowitz O, Parry PV, Hadelsberg U, Kano H, Niranjan A, Kondziolka D, & Lunsford LD (2013). Leukoencephalopathy after whole-brain radiation therapy plus radiosurgery versus radiosurgery alone for metastatic lung cancer. Cancer, 119(1), 226–232. [PubMed: 22707281]

3. Valk PE, & Dillon WP (1991). Radiation injury of the brain. American Journal of Neuroradiology, 12(1), 45–62. [PubMed: 7502957]

4. Mamlouk MD, Handweker J, Ospina J, & Hasso AN (2013). Neuroimaging findings of the post-treatment effects of radiation and chemotherapy of malignant primary glial neoplasms. Neuroradiol J, 26(4), 396–412. [PubMed: 24007728]

5. Buckner JC, Shaw EG, Pugh SL, Chakravarti A, Gilbert MR, Barger GR, Coons S, Ricci P, Bullard D, Brown PD, Stelzer K, Brachman D, Suh JH, Schultz CJ, Bahary J, Fisher BJ, Kim H, Murtha AD, Bell EH, Won M, Mehta MP, & Curran WJ (2016). Radiation plus Procarbazine, CCNU, and Vincristine in Low-Grade Glioma. N Engl J Med, 374:1344–55. [PubMed: 27050206]

6. Lupo JM, Molinaro AM, Essock-Burns E, Butowski N, Chang SM, Cha S, & Nelson SJ (2016). The effects of anti-angiogenic therapy on the formation of radiation-induced microbleeds in normal brain tissue of patients with glioma. Neuro-Oncology, 18(1), 87–95. [PubMed: 26206774]

7. Wahl M, Anwar M, Hess CP, Chang SM, & Lupo JM (2017) Relationship between radiation dose and microbleed formation in patients with malignant glioma. Radiat Oncol, 12, 126 [PubMed: 28797254]

8. Lupo JM, Chuang CF, Change SM, Barani IJ, Jimenez B, Hess CP, & Nelson SJ (2012). 7 Tesla Susceptibility-Weighted Imaging to Assess the Effects of Radiation Therapy on Normal Appearing

Brain in Patients with Glioma. Int J Radiat Oncol Biol Phys, 82(3), e493–e500. [PubMed: 22000750]

9. Roddy E, Sear K, Felton E, Tamrazi B, Gauvain K, Torkildson J, Del Buono B, Samuel D, Hass-Kogan DA, Chen J, Goldsby RE, Banderjee A, Lupo JM, Molinaro AM, Fullerton HJ, & Mueller S (2016). Presence of cerebral microbleeds is associated with worse executive function in pediatric brain tumor survivors. Neuro Oncol. 18(11), 1548–1558. [PubMed: 27540084]

10. Li X, Yuan J, Yang L, Qin W, Yang S, Li Y, Fan H, & Hu W (2017). The significant effects of cerebral microbleeds on cognitive dysfunction: An updated meta-analysis. PLoS One. 12(9), e0185145 [PubMed: 28934304]

11. Bian W, Hess CP, Chang SM, Nelson SJ, & Lupo JM (2014). Susceptibility-weighted MR Imaging of Radiation Therapy- induced Cerebral Microbleeds in Patients with Glioma: A Comparison Between 3T and 7T. Neuroradiology, 56, 91–96. [PubMed: 24281386]

12. Bian W, Banerjee S, Kelly DAC, Hess CP, Larson PEZ, Chang SM, Lupo JM (2015). Simultaneous imaging of radiation-induced cerebral microbleeds, arteries and veins, using a multiple gradient echo sequence at 7 Tesla. J Magn Reson Imaging, 42(2), 269–279. [PubMed: 25471321]

13. Lupo JM, Banerjee S, Hammond KE, Kelley DAC, Xu D, Chang SM, Vigneron DB, Majumdar S, Nelson SJ (2009). GRAPPA-based Susceptibility-Weighted Imaging of Normal Volunteers and Patients with Brain Tumor at 7T. Magn Reson Imaging, 27(4), 480–488 [PubMed: 18823730]

14. Wen Q, Kelley DAC, Banerjee S, Lupo JM, Chang SM, Xu D, Hess CP, & Nelson SJ (2015). Clinically feasible NODDI characterization of glioma using multiband EPI at 7 T. NeuroImage: Clinical, 9(2015), 291–299. [PubMed: 26509116]

15. Bian W, Hess CP, Chang SM, Nelson SJ, & Lupo JM (2013). Computer-aided detection of radiation-induced cerebral microbleeds on susceptibility-weighted MR images. NeuroImage: Clinical, 2(1), 282–290. [PubMed: 24179783]

16. Morrison MA, Payabvash S, Chen Y, Avadiappan S, Shah M, Zou X, Hess CP, & Lupo JM (2018). A user-guided tool for semi-automated cerebral microbleed detection and volume segmentation: evaluating vascular injury and data labelling for machine learning. NeuroImage: Clinical, 20, 498–505. [PubMed: 30140608]

17. van den Heuvel TL, van der Eerden AW, Manniesing R, Ghafoorian M, Andriessen TM, Vande Vyvere T, van den Hauwe L, Ter Haar Romeny BM, Goraj BM, & Platel B (2016). Automated detection of cerebral microbleeds in patients with Traumatic Brain Injury. Neuroimage Clinical, 2(12), 241–251.

18. Belliveau JG, Baumen GS, Tay KY, Ho D, & Menon RS (2017). Initial Investigation into Microbleeds and White Matter Signal Changes following Radiotherapy for Low-Grade and Benign Brain Tumors Using Ultra-High-Field MRI Techniques. AJNR, 38(12), 2251–2256. [PubMed: 28970242]

19. Yeom KW, Lober RM, Partap S, Telischak N, Tsolinas R, Barnes PD, & Edwards MS (2013). Increased focal hemosiderin deposition in pediatric medulloblastoma patients receiving radiotherapy at a later age. J Neurosurg Pediatr, 12(5), 444–451. [PubMed: 23992236]

20. Roongpiboonsopit D, Kuijf H, Lily A, Charidimou A, Xiong L, Vashkevich A, Martinez-Ramirez S, Shih H, Gill CM, Viswanathan A, & Dietrich J, (2017). Evolution of Cerebral Microbleeds After Cranial Irradiation in Medulloblastoma Patients. Neurology, 88(8): 789–796. [PubMed: 28122904]

21. Poels MM, Ikram MA, van der Lugt A, Hofman A, Niessen WJ, Krestin GP, Breteler MMB, & Vernooij MW (2012). Cerebral microbleeds are associated with worse cognitive function: The Rotterdam Scan Study. Neurology, 78(5): 326–333. [PubMed: 22262748]

22. Liebeskind DS, Sanossian N, Sapo ML, & Saver JL (2013). Cerebral Microbleeds After Use of Extracorporeal Member Oxygenation in Children. J Neuroimaging, 23(1), 75–78. [PubMed: 22606942]

23. Bradley WG (1993). MR Appearance of Hemorrhage in the Brain. Radiology, 189(1), 15–26. [PubMed: 8372185]

24. Liu W, Soderlund K, Senseney JS, Joy D, Ping-Hong Y, Ollinger J, Sham EB, Liu T, Wang Y, Oakes TR, & Riedy G (2016). Imaging Cerebral Microhemorrhages in Military Service Members with Chronic Traumatic Brain Injury. Radiology, 278(2), 536–545. [PubMed: 26371749]

25. Lawrence TP, Pretorius PM, Ezra M, Cadoux-Hudson T, & Voets NL (2017). Early detection of cerebral microbleeds following traumatric brain injury using MRI in the hyper-acute phase. Neuroscience Letters, 655(2017), 143–150. [PubMed: 28663054]

26. Watanabe J, Maruya J, Kanemaru Y, Miyauchi T, & Nishimaki K (2016). Transient disappearance of microbleeds in the subacute period based on T2*-weighted gradient echo imaging in traumatic brain injury. Acta Neurochir, 158(2016), 1247–1250. [PubMed: 27106841]

27. Burzynska AZ, Jiao Y, Knecht AM, Fanning J, Awick EA, Chen T, Gothe N, Voss MW, McAuley E, & Kramer AF (2017). White matter integrity declined over 6-months, but Dance intervention improved integrity of the fornix in older adults. Frontiers in Aging Neuroscience, 9(59), 1–15. [PubMed: 28174533]

28. Nagesh V, Tsien CI, Chenevery TL, Ross BD, Lawrence TS, Junck L, & Cao Y (2008). Radiation-Induced Changes in Normal Appearing White Matter in Patients with Cerebral Tumors: A Diffusion Tensor Imaging Study. Int J Radiat Oncol Biol Phys, 70(4), 1002–1010. [PubMed: 18313524]

29. Kassubek R, Gorges M, Westhoff M, Ludolph AC, Kassubek J, & Muller H (2017). Cerebral Microstructural Alterations after Radiation Therapy in High-Grade Glioma: A Diffusion Tensor Imaging-Based Study. Front Neurol, 8(2017), 286. [PubMed: 28663738]

30. Hope T, Varal J, Bjornerud A, Larsson C, Arnesen MR, Salo RA, & Groote IR (2015). Serial diffusion tensor imaging for early detection of radiation-induced injuries to normal-appearing white matter in high-grade glioma patients. J Magn Reson Imaging, 41(2), 414–423. [PubMed: 24399480]

31. Mabbott DJ, Noseworthy MD, Bouffet E, Rockel C, & Laughlin S (2006). Diffusion tensor imaging of white matter after cranial radiation in children for medulloblastoma: Correlation with IQ. Neuro-Oncology, 8(3), 244–252. [PubMed: 16723629]
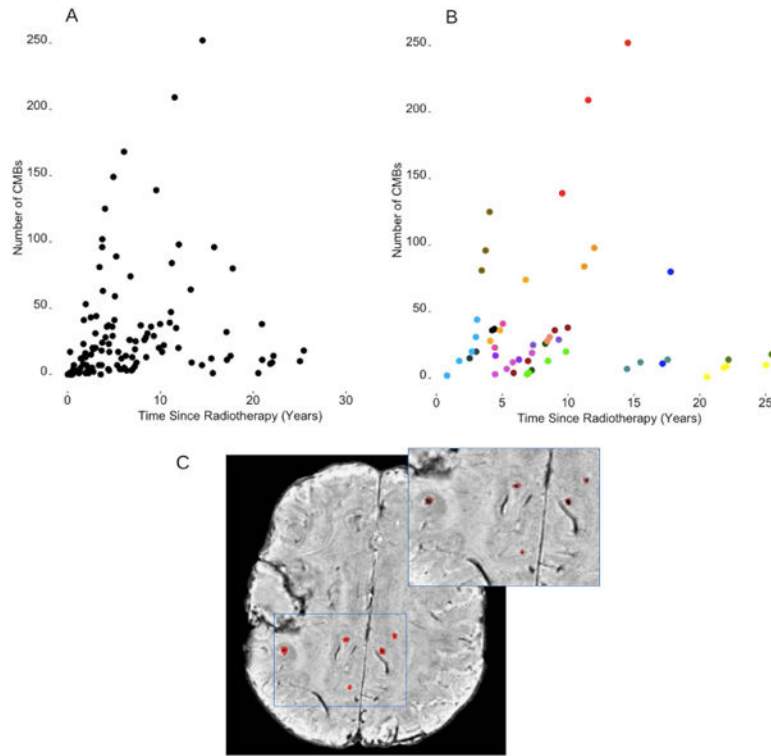
Figure 1.
Total number of CMBs as a function of time since radiotherapy in all patients treated with RT (*panel A*) and in those patients who underwent serial imaging (*panel B*). Each data point corresponds to a single imaging time point. In panel B, different colors correspond to different patients. Panel C illustrates one representative patient case of candidate CMBs labeled on a non-projected SWI axial image slice. The surgical cavity in the right hemisphere containing unrelated blood product that has been excluded from the analysis. The blue outlined region of interest is magnified in the top right corner for better visualization.
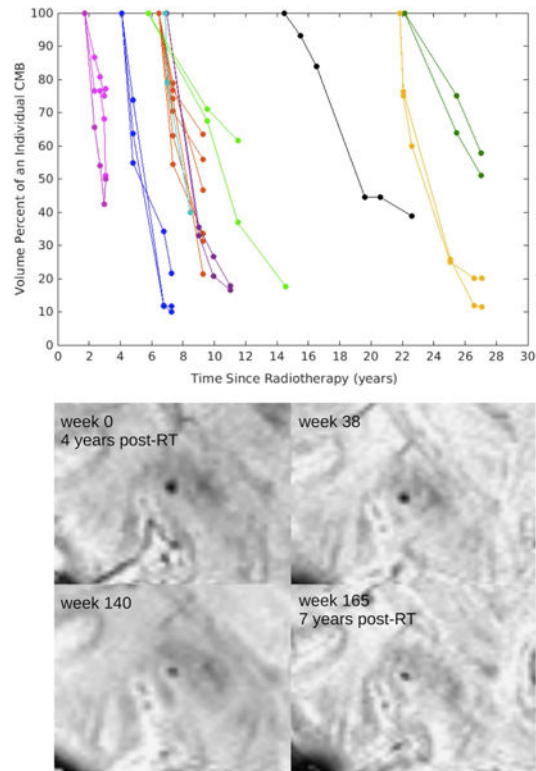
Figure 2.
Above: Decreasing CMB volume over time. Change in CMB volume percent over time. Each line color corresponds to a different patient and each line corresponds to an individual CMB tracked over multiple time points. *Below*: Example of one CMB decreasing in size over a 3-year period in a representative patient.
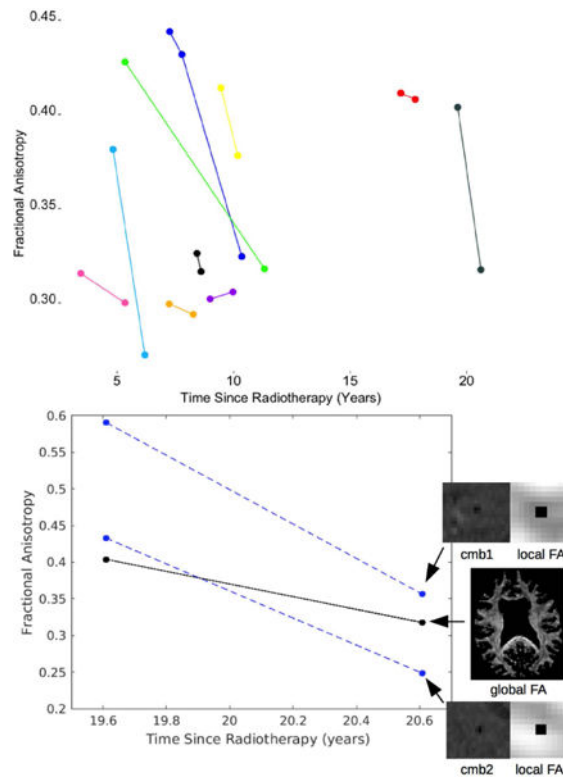
Figure 3.
Serial changes in white matter FA. *Above*: global changes in FA shown for 10 patients.
Below: global and local changes shown for 1 representative patient.

Table 1.

Patient Demographics.

Clinical/Demographic Characteristics	Proportion of Patients	
	$N_{tot} = 91$	$N_{RT} = 22$
Female (%)	30 (33.0)	8 (36.4)
Race (%)		
White	66 (72.5)	18 (81.8)
Black	2 (2.2)	0 (0)
Asian	8 (8.8)	1 (4.6)
Other	14 (15.4)	3 (13.6)
Unknown	1 (1.1)	0 (0)
Tumor pathology (%)		
WHO I Pilocytic Astrocytoma	1 (1.1)	1 (4.5)
WHO II Oligodendroglioma	7 (7.7)	5 (22.8)
WHO II Astrocytoma	8 (8.8)	7 (31.8)
WHO II Oligoastrocytoma	2 (2.2)	2 (9.1)
WHO III Anaplastic Oligodendroglioma	11 (12.1)	2 (9.1)
WHO III Anaplastic Astrocytoma	14 (15.4)	0 (0)
WHO III Oligoastrocytoma	4 (4.4)	1 (4.5)
WHO IV Glioblastoma	33 (36.2)	2 (9.1)
Other	11 (12.1)	2 (9.1)
Tumor location (%)		
Frontal	46 (50.5)	11 (50.0)
Temporal	19 (20.9)	4 (18.3)
Parietal	6 (6.6)	2 (9.1)
Frontotemporal	5 (5.5)	1 (4.5)
Frontoparietal	4 (4.4)	1 (4.5)
Occipital, Cerebellum or Brainstem	7 (7.7)	1 (4.5)
Other	4 (4.4)	2 (9.1)
Radiation (%)	91 (100)	-
>1 treatment due to recurrence	9 (9.9)	-
Age at radiation therapy, median (range)	44 (26-73)	-
Chemotherapy (%)	81 (89.0)	10 (45.5)
Time since RT, year median (range)	5.33 (.02 - 35)	-
Surgical resection (%)	77 (84.6)	21 (95.4)
>1 surgery due to recurrence	21 (23.1)	8 (36.4)

Table 2.

Multivariate analysis of risk factors for CMB burden.

Risk factors for CMB development				
	Univariate Poisson Analysis		**Multivariate Poisson Analysis**[a]	
Characteristic	**Incidence Rate Ratio**	**P-value**	**Incidence Rate Ratio**	**P-value**
Time since RT, each additional year	1.05 (1.02, 1.09)	<.001	1.10 (1.04, 1.16)	<.001
>1 surgical resection	1.98 (1.12, 3.51)	.022	2.42 (1.36, 4.30)	.004
Tumor pathology				
Glioblastoma vs anaplastic astrocytoma	2.69 (1.29, 5.61)	.010	2.41 (1.21, 4.77)	.014
Glioblastoma vs other	1.25 (.464, 3.37)	.661	.257 (.064, 1.04)	.060
Tumor location				
Frontal vs temporal	.454 (.188, 1.10)	.083	.445 (.213, .932)	.035
Frontal vs parietal	.353 (.066, 1.87)	.225	.204 (.046, .900)	.039
Frontal vs occipital, cerebellum or brainstem	1.11 (.413, 2.97)	.840	3.58 (1.20, 10.6)	.025
Maximum brain radiation, each additional Gy[b]	1.00 (.999,1.00)	.579	not included as significant	
Type of SWI acquired				
Multi-echo vs single-echo SWI[c]	.534 (.291, .980)	.046	.717 (.425, 1.21)	.217

[a] race, sex, and age at time of RT included as covariates.

[b] 37 subjects

[c] difference in slice thickness: 1mm for single echo SWI and 2mm for multi-echo SWI.

Table 3.

Multivariate analysis of serial changes in CMB burden.

Serial changes in CMB burden		
	Multivariate Poisson Analysis	
Total CMB count, time since RT[b]	1.18 (1.14, 1.22)	<.001
Total CMB volume, time since RT[b]	1.11 (1.09, 1.13)	<.001
Individual CMB volume, time since RT[c]	.750 (.699, .806)	<.001

[a] race, sex, and age at time of RT included as covariates.

[b] 19 subjects, 53 observations

[c] 8 subjects, 79 observations